

# Photonic crystal structures with ultrahigh aspect ratio in lithium niobate fabricated by focused ion beam milling

Guangyuan Si and Aaron J. Danner<sup>a)</sup>

*Centre for Optoelectronics, Department of Electrical and Computer Engineering, National University of Singapore, 4 Engineering Drive 3, Singapore 117576*

Siew Lang Teo, Ee Jin Teo, and Jinghua Teng<sup>b)</sup>

*Institute of Materials Research and Engineering, 3 Research Link, Singapore 117602*

Andrew A. Bettiol

*Centre for Ion Beam Applications, Department of Physics, National University of Singapore, 2 Science Drive 3, Singapore 117542*

(Received 28 November 2010; accepted 21 January 2011; published 3 March 2011)

Lithium niobate ( $\text{LiNbO}_3$ , LN) is an important material which is widely applied in fabricating photonic and acoustic devices. However, it is difficult to either wet etch or dry etch LN due to the material's properties. Here, the authors report novel pattern fabrication based on LN using focused ion beam (FIB) milling. When an array of small holes is etched, a severe tapering problem is observed as is common, but by replacing the nanocylindrical hole array with a nanoring structure, the authors obtain photonic crystals with an aspect ratio of up to 50:1 (2  $\mu\text{m}$  total etching depth and 40 nm gap aperture). Dense nanorod arrays with sub-30-nm ultrasmall gaps and more than 2.5  $\mu\text{m}$  etching depth are also achieved with FIB milling. © 2011 American Vacuum Society. [DOI: 10.1116/1.3557027]

## I. INTRODUCTION

Lithium niobate ( $\text{LiNbO}_3$ , LN) has drawn considerable attention because of its various useful optical properties. It is extensively used in nonlinear optical, piezoelectric, and photorefractive devices. Waveguides in LN are used for high-speed modulation or for nonlinear devices such as parametric oscillators and amplifiers. LN is also common in telecommunication systems due to its high electro-optical coefficient and low optical losses. LN is notoriously difficult to etch, however, and the fabrication of various waveguide structures such as right-angle bends,  $T$ -junctions, and photonic crystals (PCs) typically requires the use of high-index contrast structures. Such structures require robust LN etch processes. PCs, for example, offer the possibility of realizing high-density integrated optical systems but are among the most difficult to fabricate in LN.

The fabrication of LN PCs would provide a way of significantly decreasing the size of crucial LN components in optical communication systems, which are generally quite large due to the use of diffused waveguides when fabricated in LN. Since LN exhibits a strong Pockels effect, tunability of PCs could be achieved simply by applying electric fields resulting in fast switching.<sup>1,2</sup> Focused ion beam (FIB) lithography is a frequently used technique to fabricate PCs in LN.<sup>3,4</sup> Since PCs require vertical optical confinement, a potential approach for achieving this in LN would be to implant a bulk LN sample followed by thin film transfer (crystal ion slicing and wafer bonding).<sup>5,6</sup> Fabrication of suspended slab and PC waveguides by implantation and wet etching has also

been investigated previously.<sup>7</sup> Therefore, it is worth investigating dry etching methods in LN for creating lateral index steps which are useful for a wide range of devices.

The FIB instrument is a useful tool based on ion beam-solid interactions.<sup>8</sup> Equipped with a liquid ion source (Ga, normally), it can define patterns directly without using masks. In addition, since FIB lithography can be applied to almost all materials, it has found extensive applications in manufacturing semiconductor devices.<sup>9,10</sup> Due to its versatile and reliable properties, fabrication of three-dimensional structures was also achieved.<sup>11,12</sup>

In this article, we demonstrate improving the profiles of PC structures by developing different patterns using FIB lithography. Nanorings with over 50:1 aspect ratio are realized. All patterns are fabricated with good uniformity and high homogeneity. Furthermore, nanorod crystals are fabricated by increasing the outer radii of ring structures and realigning the ring array patterns as will be described. Ultrasmall gaps with less than 30 nm width are also achieved. Gap apertures can be simply tuned by varying the overlapping area.

## II. NANOHOLE WITH STANDARD PROFILES

A common problem of using FIB milling methods is conical sidewalls, caused by redeposition during etching which is inevitable. Straight sidewalls are preferred. To demonstrate the redeposition effect, we start with a typical two-dimensional planar PC structure. 100 nm Au with 5 nm Ti as adhesion layer was first deposited on an  $x$ -cut LN sample surface by electron beam evaporation to avoid charging problems during FIB milling. Then all the hole patterns were milled in parallel to minimize the redeposition effect using a

<sup>a)</sup>Electronic address: adanner@nus.edu.sg

<sup>b)</sup>Electronic address: jh-teng@imre.a-star.edu.sg

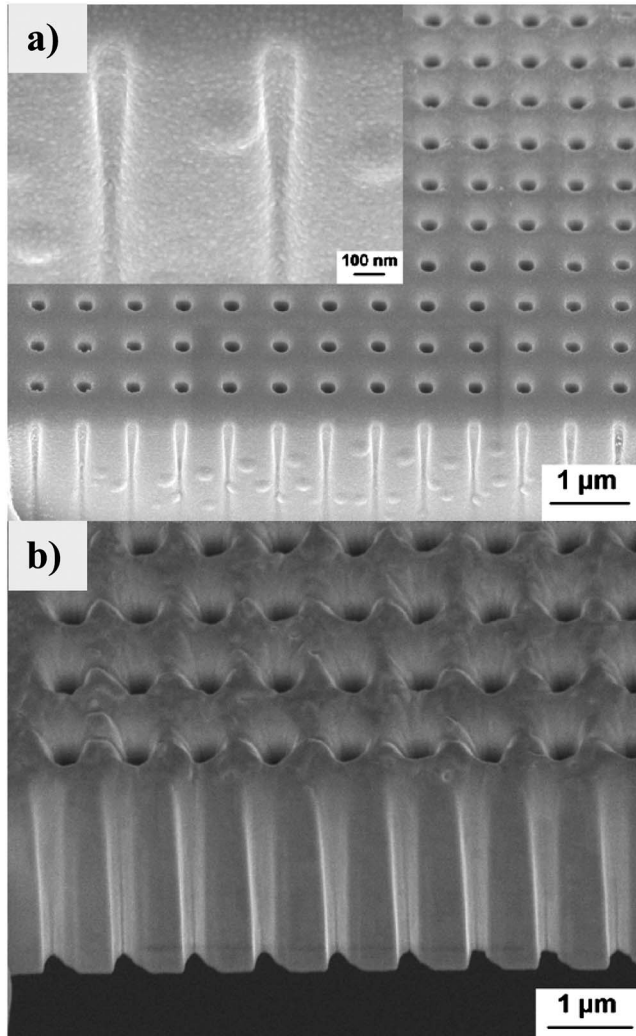


FIG. 1. (a) Scanning electron micrograph (SEM) image showing the tapered cross sections of nanoholes. (b) Cross section of PCs in a suspended LN film fabricated by implantation, FIB milling, and wet etching.

70 pA probe current with a 30 kV acceleration voltage to achieve patterns with high uniformity. The metals on sample surface also function as protective layer during scanning and milling to minimize ion damage to the LN surface. One should also note that it is easy to remove all redeposited materials after milling by simply removing the metals on a sample surface using wet etching to obtain a clean LN face.

Figure 1(a) shows a typical cross-sectional profile of nanoholes fabricated in a LN sample by FIB milling. From the inset of Fig. 1(a), we can observe profiles with a serious tapering shape which is common in FIB milling due to material redeposition. One can also find bubbles interspersed among the sidewalls. Conical profiles could affect optical device performance dramatically, so this represents a serious problem as large optical losses may be caused.<sup>13,14</sup> One potential solution is to truncate the tapered bottoms to minimize the impact generated by gradient shapes by making the holes

suspended using combined techniques of implantation, FIB milling, and wet etching as shown in our previous work.<sup>7</sup> Figure 1(b) demonstrates the cross section of PCs fabricated in a suspended LN film with severely tapered bottoms truncated using combined techniques mentioned above. One can find significantly improved profiles of the cylindrical structures. Nonetheless, simply etching holes will always result in a conical profile. As will be described, other shapes do not necessarily suffer from the same effect.

### III. NANORINGS WITH ULTRAHIGH ASPECT RATIO

To further investigate the feasibility of fabricating high aspect ratio PCs with homogeneous etching profiles, we developed coaxial ringlike structures by direct FIB patterning. As illustrated in Fig. 2, a series of two-lattice superimposed PCs with fixed inner radius (nominally 80 nm) and varying outer radii (140–260 nm in 40 nm increments) was fabricated. Different effective indices can be generated simply by varying inner nanorod diameters and surrounding air filling factors of the rings. The spot size of an ion beam is determined by many factors, such as dwell time, beam overlap, focus, stigmatism, and especially probe current. Taking both the total etching time and desired features into account, an 11 pA probe current was selected to mill the ring patterns in this work. This corresponds to a 15 nm spot diameter. The total milling time for a  $9 \times 9$  ring array was approximately 5 min. By replacing the nanoholes described in Sec. II with ring structures, we can improve the milled profiles remarkably and uniform cross sections can be obtained with a high aspect ratio. As demonstrated in Fig. 3, nanorings with a 40 nm gap aperture (200 nm inner radius and 240 nm outer radius) exhibit good uniformity with 50:1 aspect ratio (over 2  $\mu\text{m}$  total etching depth). We observe straight ring apertures as shown in the cross-sectional view in Fig. 3(b). Since postetch FIB cross sectioning processes can cause etches to appear deeper than they actually are (phantom etches) during the cross sectioning process, these were also investigated in Sec. III to ensure that the aspect ratio was not a FIB cross sectioning artifact and was truly a result of the initial FIB milling.

In addition, one can control the aspect ratio by simply varying the geometry of the ring arrays to make PC structures with different effective indices for various applications. It appears that ring shapes are much more resistant to the tapering effect than standard holes, and this is the primary motivation for this report, as this property may be important for fabrication of various nanoscale devices with FIB milling.

The conical cross-sectional profiles are mainly caused by redeposition problem which is inevitable during milling. Conical shaped holes will generate high optical losses and they could hardly produce well-defined stop bands in the transmission spectra. One proposed solution is to truncate the

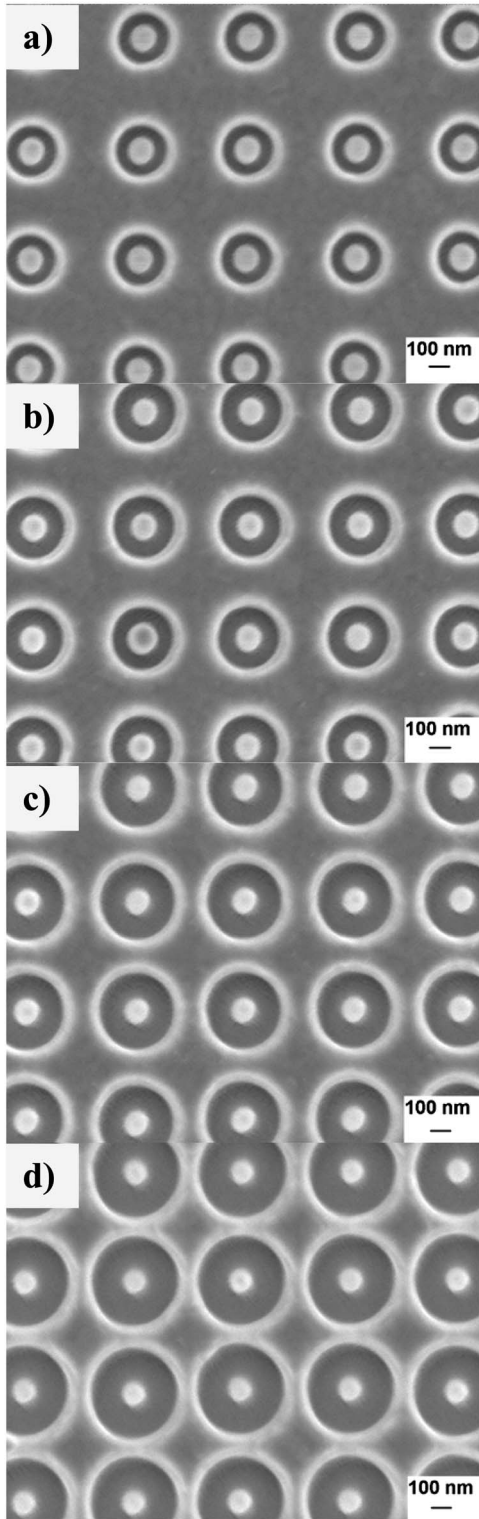


FIG. 2. Top view SEM images of superimposed PCs of various effective indices achieved by geometry tuning. The ring structures have fixed inner radius (80 nm) and varying outer radii: (a) 140 nm, (b) 180 nm, (c) 220 nm, and (d) 260 nm.

tapered bottoms and reshape the cross sections using appropriate techniques. Another potential approach is to replace cylindrical holes with coaxial structures which have been studied for decades.<sup>15,16</sup> More beam energy can be concen-

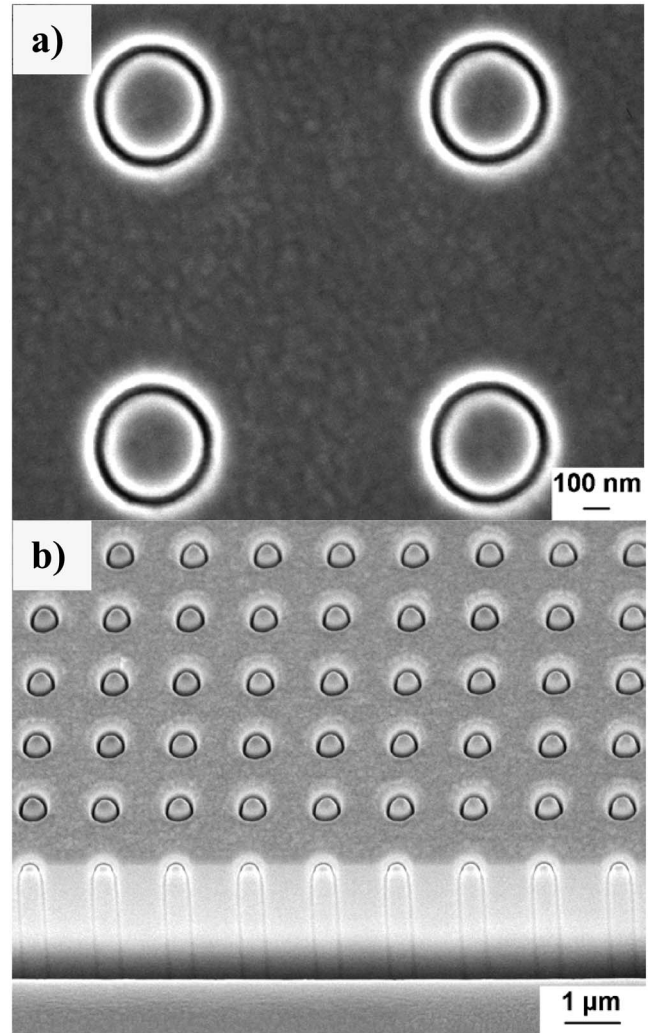


FIG. 3. (a) Top view of the nanoring arrays with 200 nm inner radius and 240 nm outer radius. (b) Cross sectional view showing the straightly etched ring apertures.

trated in the ring area which results in reduced energy spread and total etching time during the FIB process, enabling small features and large etching depth simultaneously. In all-dielectric coaxial frames, polarization can be maintained throughout propagation due to the radially symmetric electric field distribution. Moreover, coaxial geometries can be used to guide light around sharp bends since the radial confinement of the light is a consequence of omnidirectional reflection instead of total internal reflection.<sup>17</sup> Coaxial holes can also be used to create PC structures with similar characteristics to those of standard air hole PCs.<sup>18</sup> They have been used to create waveguides with polarization-independent guiding effect<sup>19</sup> and a complete photonic band gap<sup>20,21</sup> most recently. More designs and fabrication work have been investigated elsewhere.<sup>22,23</sup>

#### IV. NANOROD CRYSTALS BY FIB MILLING

By further increasing the outer radii and realigning the ring arrays, we can obtain nanorods with different shapes by FIB milling. Figure 4 shows a glancing view of dense nano-

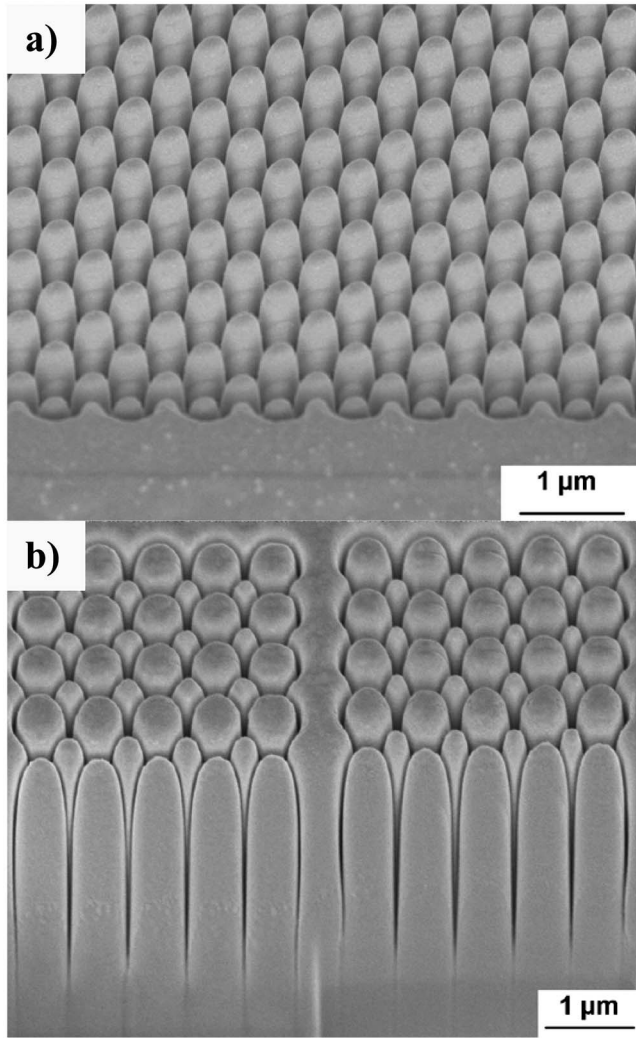


FIG. 4. (a) Glancing view of nanorod arrays with hexagon-shaped lattices. (b) Cross sectional view showing the bottoms of nanorods using a gradient milling at  $15^\circ$  tilting angle.

rod arrays with different lattices. Although we can observe coniform tops for the nanorods, gaps between individual crystals become uniform from 500 nm downward. The coniform tops are caused by damage during long-time milling and scanning when adjusting system parameters to focus and viewing. Since a single beam FIB system (FIB 200, FEI Company) was employed in this work, we tried to reduce scanning time to minimize ion damage during navigation to a target region but some damage was unavoidable. There are no such problems for dual-beam (electron and ion sources) FIB systems because navigation can be performed using the electron beam instead. One should also note that the damage for the patterns (especially the top parts) becomes severe as the milling time is extended (for deep etching) which could cause cone-shaped profiles as well. To present the bottoms of the nanorods without showing any artifacts caused by FIB cross sectioning, a gradient milling at  $15^\circ$  tilting angle was applied to the rod bottom parts as illustrated in Fig. 4(b). This shows the true etching depth achieved during initial

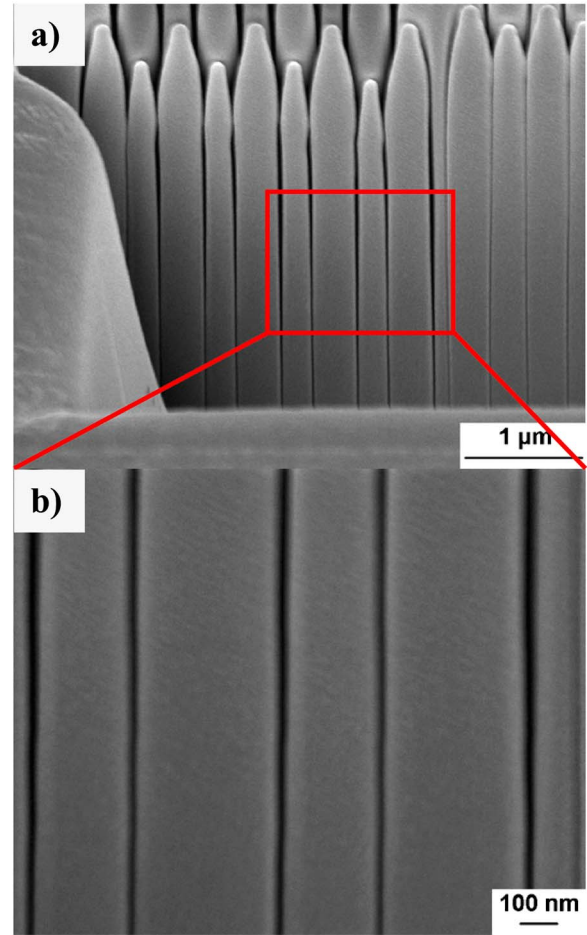


FIG. 5. (Color online) (a) Low and (b) high magnification cross-sectional images showing vertically etched dense nanorods with less than 30 nm gaps and more than  $2.5 \mu\text{m}$  etching depth.

milling by eliminating any potential additional vertical etching during the cross sectioning process. The aspect ratio reported above is repeated and thus verified.

The FIB technique is a maskless lithography method since ions can directly define patterns on a wide range of materials. In addition, without producing forwardscattering and backscattering, a fine defined ion beam is capable of fabricating narrow linewidths and structures at nanoscale with high aspect ratio and accuracy. In this work, nanocavities obtained using such a method have ultrasmall gaps with quite a large etching depth. As shown in Fig. 5, dense pillar arrays have been fabricated with less than 30 nm gaps and ultrahigh aspect ratios (more than  $2.5 \mu\text{m}$  etching depth).

## V. CONCLUSION

To conclude, we have investigated conical profiles of FIB milling method caused by redeposition. By applying ring-pattern milling instead of simple hole milling, ultrahigh aspect ratio over 50:1 has been observed. Once the ion energy is focused onto a smaller milling area on sample surface, dry etching can go much deeper with significantly reduced total milling time using a well-defined ion beam. Moreover, nanorod arrays with sub-30-nm cavity gaps have been fabricated

using an improved and realigned ring-pattern milling function. Different geometries with various lattice shapes are available in bulk LN now. Most importantly, one can tune the effective indices more efficiently since both of the inner nanorod diameter and the outer surrounding air filling factor are controllable. Fabrication of homogeneous PCs enables a new series of optical devices which can be easily applied to bulk LN.

## ACKNOWLEDGMENT

The authors gratefully acknowledge financial support from NUS Cross Faculty Grant No. R263000529646.

<sup>1</sup>M. Roussey, M.-P. Bernal, N. Courjal, D. Van Labeke, F. I. Baida, and R. Salut, *Appl. Phys. Lett.* **89**, 241110 (2006).

<sup>2</sup>M. Roussey, F. I. Baida, and M.-P. Bernal, *J. Opt. Soc. Am. B* **24**, 1416 (2007).

<sup>3</sup>F. Chen, *J. Appl. Phys.* **106**, 081101 (2009).

<sup>4</sup>F. Lacour, N. Courjal, M.-P. Bernal, A. Sabac, C. Bainier, and M. Spajer, *Opt. Mater. (Amsterdam, Neth.)* **27**, 1421 (2005).

<sup>5</sup>M. Levy, R. M. Osgood, Jr., R. Liu, L. E. Cross, G. S. Cargill III, A. Kumar, and H. Bakhru, *Appl. Phys. Lett.* **73**, 2293 (1998).

<sup>6</sup>A. Guarino, G. Poberaj, D. Rezzonico, R. Degl'Innocenti, and P. Günter, *Nat. Photonics* **1**, 407 (2007).

<sup>7</sup>G. Si, E. J. Teo, A. A. Bettiol, J. Teng, and A. J. Danner, *J. Vac. Sci. Technol. B* **28**, 316 (2010).

<sup>8</sup>*Focused Ion Beam Systems: Basics and Applications*, edited by N. Yao (Cambridge University Press, Cambridge, 2007).

<sup>9</sup>C. R. Musil, J. Melngailis, S. Etchin, and T. E. Haynes, *J. Appl. Phys.* **80**, 3727 (1996).

<sup>10</sup>C. Crell, S. Friedrich, H.-U. Schreiber, and A. D. Wieck, *J. Appl. Phys.* **82**, 4616 (1997).

<sup>11</sup>M. J. Vasile, Z. Niu, R. Nassar, W. Zhang, and S. Liu, *J. Vac. Sci. Technol. B* **15**, 2350 (1997).

<sup>12</sup>S. Matsui, T. Kaito, J. Fujita, M. Komuro, K. Kanda, and Y. Haruyama, *J. Vac. Sci. Technol. B* **18**, 3181 (2000).

<sup>13</sup>Y. Tanaka, T. Asano, Y. Akahane, B.-S. Song, and S. Noda, *Appl. Phys. Lett.* **82**, 1661 (2003).

<sup>14</sup>G. W. Burr, S. Diziain, and M.-P. Bernal, *Opt. Express* **16**, 6302 (2008).

<sup>15</sup>R. DeVore, J. F. Toth, and R. Caldecott, *J. Appl. Phys.* **44**, 4488 (1973).

<sup>16</sup>R. DeVore, *J. Appl. Phys.* **45**, 2874 (1974).

<sup>17</sup>M. Ibanescu, Y. Fink, S. Fan, E. L. Thomas, and J. D. Joannopoulos, *Science* **289**, 415 (2000).

<sup>18</sup>H. Kurt and D. S. Citrin, *Opt. Express* **13**, 10316 (2005).

<sup>19</sup>A. Cicek and B. Ulug, *Opt. Express* **17**, 18381 (2009).

<sup>20</sup>H. Kurt, R. Hao, Y. Chen, J. Feng, J. Blair, D. P. Gaillot, C. Summers, D. S. Citrin, and Z. Zhou, *Opt. Lett.* **33**, 1614 (2008).

<sup>21</sup>P. Shi, K. Huang, X. Kang, and Y. Li, *Opt. Express* **18**, 5221 (2010).

<sup>22</sup>A. Säynätjoki, M. Mulot, J. Ahopelto, and H. Lipsanen, *Opt. Express* **15**, 8323 (2007).

<sup>23</sup>J. Feng, Y. Chen, J. Blair, H. Kurt, R. Hao, D. S. Citrin, C. J. Summers, and Z. Zhou, *J. Vac. Sci. Technol. B* **27**, 568 (2009).